Optimizing Beam Profiles for Polar Drive Implosions on the National Ignition Facility

Felix Weilacher

Penfield High School

Penfield, New York

Advisor: Radha Bahukutumbi

Laboratory for Laser Energetics

University of Rochester

Rochester, New York

August 29th, 2014

Abstract

In polar drive (PD) geometry, beams are displaced closer to the equator from their original on-target positions to achieve better implosion symmetry. Current direct-drive polar drive implosions for the National Ignition Facility (NIF) use phase plates - optics which define the shape of the laser beams or beam profiles - designed for indirect drive. The uniformity achieved in PD implosions is therefore limited. Optimal laser beam profiles have been identified using the hydrodynamics code DRACO. A combination of spherically symmetric and elliptical beam profiles are necessary for nearly uniform implosions. With the use of these optimized beam profiles, adjustments to laser temporal power histories can significantly improve symmetry and therefore target performance. These optimal beam profiles are also robust to model variations. For example, the same beam profiles can be used to optimize designs with different heat conduction models by requiring a relatively minor variation in laser power histories. The neutron yield increases by ~50% compared to designs using current NIF profiles.

I. Introduction

In inertial confinement fusion (ICF),[1] many nominally identical laser beams are incident on a shell made of materials such as plastic containing a layer of solid cryogenic deuterium-tritium. This irradiation causes ablation of the outer regions of the target, driving the rest of the shell inward like a rocket.

A couple of different methods of delivering energy to the surface of the target are currently possible on laser facilities: direct drive,[1,2] where beams illuminate a target directly

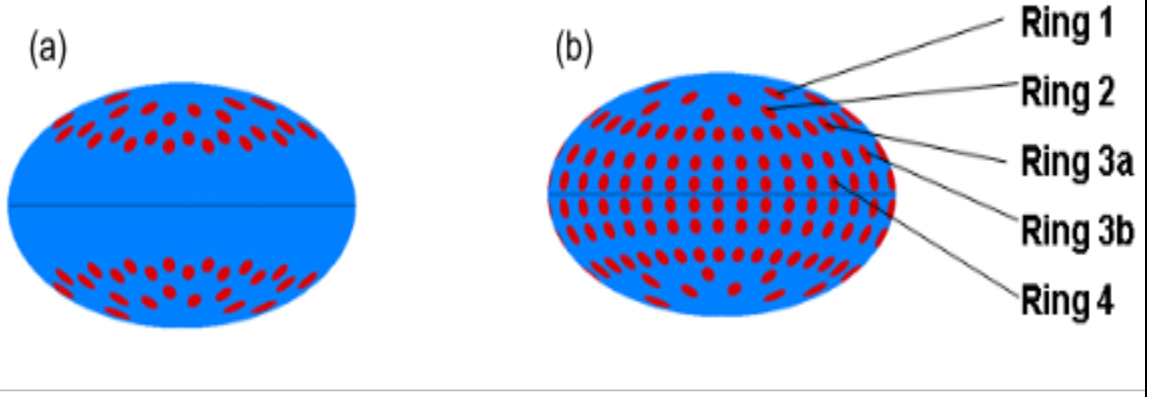

Figure 1: (a) Original NIF beam pointing configuration. (b) Optimized polar drive beam pointings. Note that Ring 3 is split into two rings and that the quads of rings 3 and 4 are split in the azimuthal direction.

from all sides, and indirect drive,[3] where a target is placed inside a hohlraum (a gold cylindrical capsule with holes at the ends) and beams illuminate the sides of this hohlraum, causing the emission of x rays which then deliver energy to the target.

On facilities configured for direct drive, such as OMEGA,[4] beams are set up so that they strike the target with a nearly spherically uniform distribution at normal angles of incidence. The uniformity in beam placement leads to high uniformity in on-target intensity and creates a highly symmetric spherical implosion. On a facility such as the National Ignition Facility[5] (NIF), which is configured primarily for indirect drive, however, beam ports are concentrated around the poles of the target, corresponding to the two ends of the hohlraum (Fig. 1a). Thus, using the NIF for direct drive without displacing the beams from their centers of normal incidence results in a distribution of beams on target which is far from uniform. The solution to this is polar drive,[6] wherein beams are displaced from their original positions on the target surface; the resultant on-target positions of the beams are shown in in Fig. 1b. On the NIF, beams are organized into logical groupings of rings as shown in Fig. 1. These rings are displaced toward the equator or “repointed” to achieve better on-target symmetry.

Since beams are displaced laterally, beams which are repointed irradiate the target at more oblique angles of incidence. This results in the laser energy being deposited further away from the ablating shell and a reduction in drive. The equatorial beams must be repointed over the greatest polar angle from their original position and beam obliquity can significantly compromise drive at the equator. Thus, polar drive implosions tend to be underdriven at the equator.

Although the use of polar drive significantly improves the uniformity of the distribution of beams, and thus of on-target intensity, additional improvements to the irradiation uniformity can be made through the optimization of the laser pulse shapes and beam profiles, two additional sets of laser parameters which are introduced below.

The target considered in this paper (shown in Fig. 2) is a 1.1 mm radius sphere with a 100 μm-thick plastic (CH) shell filled with 20 atmospheres of deuterium (D_2) gas. This is typical of targets currently being used for polar drive experiments on the NIF.

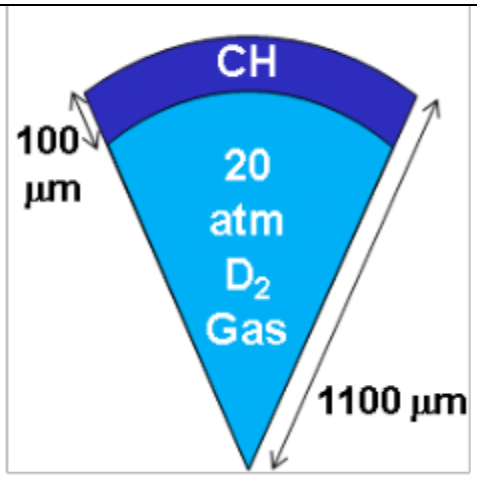

Figure 2: Cross section of a 1100 µm radius room temperature target with a 100 µm shell

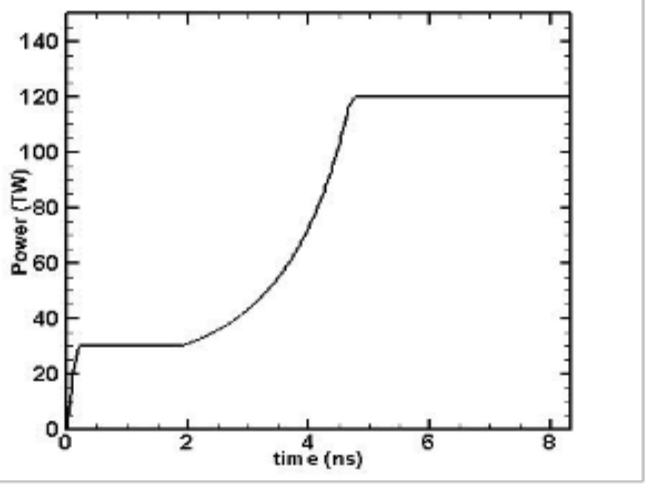

Figure 3: Example of a pulse shape, which gives laser power as a function of time over the course of an implosion. This pulse shape gives total laser power.

The design includes laser beam pulse shapes that describe the temporal power history of the beams. An example of a pulse shape is given in Fig. 3. In polar drive implosions on the NIF, these pulse shapes are characterized by a foot (between 0 and 2 ns), and then a slow rise (between 2 and 5 ns), to a main pulse (after 5ns).[7] During the initial rise to the foot a shock is launched into the shell. The length of the foot is fixed to correspond to when the shock breaks out of the shell into the gas. The overall length of the laser pulse is determined by the energy available on the laser system. Up to 700 kJ is normally available to implode a target on the NIF. Laser pulse shapes can be adjusted independently for each ring of beams, and also are easily mutable. They are thus an important tool for fine tuning polar drive implosions.

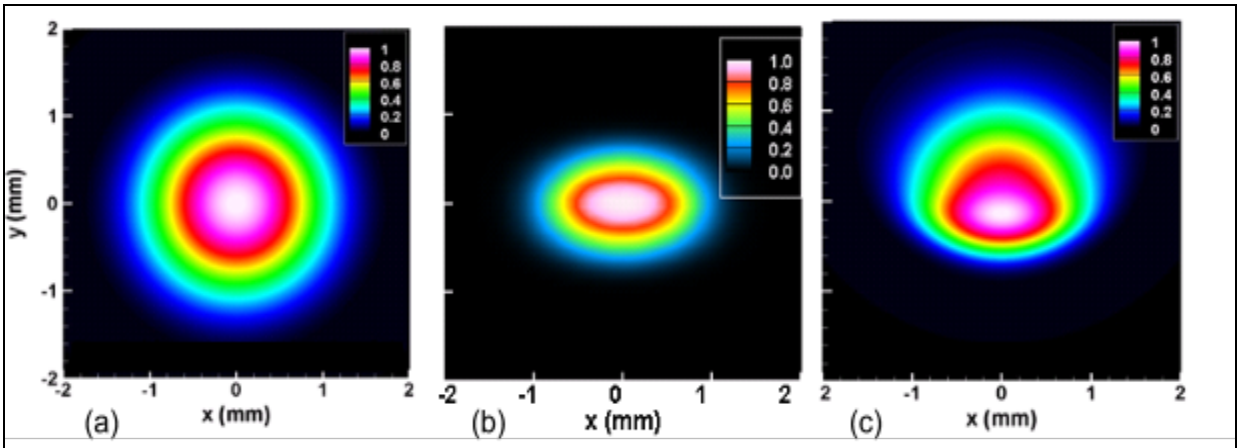

Figure 4: (a) Intensity contours of a circular beam profile. (b) Intensity contours of an elliptical beam profile. (c) Intensity contours of a profile which includes a secondary ellipse. The radius in the longest direction at 5% of peak intensity typically is equal to the target radius.

A third important set of laser parameters which can have a significant effect on the uniformity of an implosion are laser beam profiles, examples of which are shown in Figure 4. They are most intense at the center, with decreasing intensity toward the edges of the beam. The Intensity, $I(x,y)$, as a function of position for a simple, circular beam profile such as the one shown in Fig. 4a can be described as a super-Gaussian

$$I(x,y) = I_0 e^{-[(x^2+y^2)/\delta]^{n/2}} \quad [1.1]$$

where I_0 is the peak central intensity, which varies in time according to the pulse shape, δ is a constant which controls the width of the profile, and n is the super-Gaussian order. Larger values of n lead to beam profiles which are flatter at the center.

Beam profiles can take shapes with more complexity than a simple circle, however. This can have the effect of concentrating the intensity along certain directions. Fig. 4b shows an elliptical profile, given by

$$I(x,y) = I_0 e^{-[(x^2+(\eta y)^2)/\delta]^{n/2}} \quad [1.2]$$

where η is the ellipticity of the profile, defined as the ratio of the major axis to the minor axis of the ellipse. Note that elliptical beam profiles are oriented so that their major axes run latitudinally. Finally, Fig. 4c shows a complicated profile that can be described as a secondary ellipse superimposed on a primary profile;[8] this has the effect of offsetting the center of intensity from the center of the beam. This type of profile is given by

$$I(x,y) = I_0 [(1-a) e^{-[(x^2+(\eta y)^2)/\delta]^{n_1/2}} + a e^{-[(x^2+(\eta(y-o))^2)/\delta]^{n_2/2}}] \quad [1.3]$$

where o is the offset of the secondary ellipse from the center of the primary profile, and a, a fraction between 0 and 1, and $(1-a)$ define the relative intensities of the primary and secondary profiles. The ellipticity and Gaussian order for the secondary ellipse are not

necessarily the same as they are for the primary profile. These different beam profiles have advantages and disadvantages, and their merits are investigated in section II. While pulse shapes and pointings are easy to change, beam profiles are determined by phase plates, optics which are difficult and expensive to manufacture and cannot be changed.

The primary goal of this work is to identify beam profiles that can be used for experiments on the NIF devoted to studying the physics of ICF implosions. Simulations are a powerful tool to guide the design of experiments and model the conditions which predict ignition in ICF. Since the physics of laser deposition and the subsequent heat conduction to the ablation surface is extremely important to implosions, experiments are critical to test simulation codes and gain confidence in ignition predictions. Heat conduction is typically modeled using diffusion, and an empirical parameter, the flux limiter, is used to limit the simulated heat flux to match various observables in experiments. The motivation for a flux limiter is somewhat ad-hoc. An improved model in polar-drive geometry is a non-local model where heat is conducted by electrons that have long mean-free paths. It has been shown that non-local transport is an improvement over the flux-limited model based on several experiments in spherical geometry; however, rigorous comparisons with experiments in polar drive are outstanding. It is therefore critical that the experiments be designed carefully - expensive pieces of equipment such as phase plates should be robust to such uncertainties in the physics. It will be shown that the beam profiles designed in this work are robust to different models of heat conduction.

II. Simulations

Implosion simulations were carried out using the 2D hydrodynamics code DRACO[9] to determine optimal beam profiles. DRACO allows important parameters, such as beam

pointings, beam pulse shapes, and beam profiles, to be specified for all 5 rings of beams used in polar drive on the NIF and allows the effects of changes in these parameters to be tested.

Although the focus of this report is optimization of beam profiles, pointings and pulse shapes are also very important. All the simulations discussed in this report use the same polar drive pointing which gives an acceptable irradiation uniformity (Table 1). The original polar angle is shown in column 2, followed by the repointed polar angle in column 3.

Ring #	Original θ	Repointed θ
1	23.5	23.5
2	30	35
3a	44.5	49
3b	44.5	69
4	50	83

Table 1: Table showing the original and repointed polar angles for the design in this work. Rings 1 and 2 were displaced only in polar angle. Within the rings 3a, 3b, and 4, the beams were additionally moved so that they were equally spaced in the azimuthal direction.

Pulse shapes, discussed previously, are especially useful tools for fine tuning the uniformity of an implosion. The testing of various sets of beam profiles, outlined in this section, is always accompanied by adjustments to pulse shapes to identify an optimal level of uniformity. Throughout this report, when a simulated implosion using a set of beam profiles is said to have optimized pulse shapes, or to be an optimized implosion, it should be understood that there is not some universal optimal set of pulse shapes, but that pulse shapes for that implosion were tuned specifically to optimize uniformity with that set of beam profiles.

Since the NIF is designed for indirect drive, the currently installed phase plates produce elliptical beam profiles. This is because in indirect drive, beams pass through one of two laser entrance holes in the hohlraum at oblique angles. To clear a hole, the cross section

of a beam in the plane of the hole must fit the shape of the hole, which is circular. Therefore, all of the beams must be elliptically shaped. A significant interest of this work is the effect of circular beam profiles on target uniformity for polar drive ICF on the NIF when compared to these elliptical profiles.

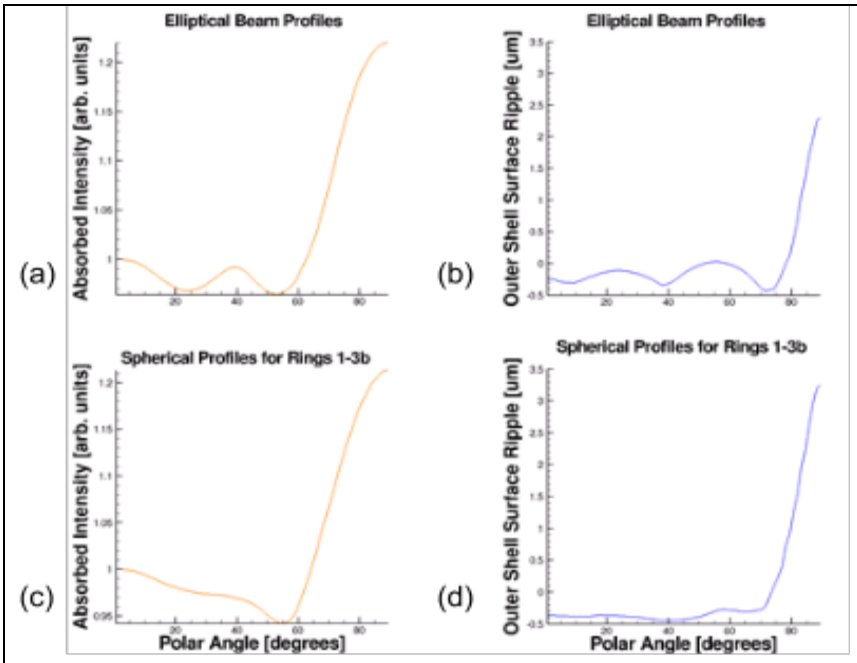

Figure 5: (a) Initial normalized on-target Intensity for an optimized implosion using elliptical beam profiles. (b) Outer shell surface position relative to the mean at 1 ns for the implosion corresponding to (a). (c) and (d) Same as (a) and (b), except for an optimized implosion using circular (spherical) beam profiles for the higher latitude rings. The pole corresponds to 0 degrees, whereas the equator is at 90 degrees.

As is shown in Fig. 4, elliptical profiles have the effect of localizing laser intensity at a specific latitude. This localization can be a useful feature, as it permits the preferential irradiation of the equator relative to the pole. An optimal set of elliptical profiles for polar drive constitutes beams with increasing ellipticities from the pole to the equator. The on-target intensity at the initial target radius at the start of an optimized simulation using these profiles is shown in Fig. 5a. The accompanying plot in Fig. 5b shows the variation in the location of the ablation surface around the average location at a time of 1 ns into that simulation (during the foot). The troughs in the irradiation pattern correspond to an underdriven outer surface. When

the higher-latitude beam profiles for Rings 1, 2, 3a and 3b are replaced with circular profiles (Fig. 5c and 5d), and pulse shapes are re-optimized, the peaks and valleys in the irradiation pattern and the ablation surface decrease in amplitude resulting in a more uniform implosion. This is due to the better overlap provided by the circular beams. Note that the equator is still significantly underdriven. This is related to the choice of the heat conduction model (all the simulations described in section II used a flux limiter model as opposed to a nonlocal model) and will be discussed in section III. Therefore, the higher latitudes, which do not require the preferential irradiation delivered by the elliptical beam profiles, can be driven more uniformly with spherical beam profiles.

The equatorial region requires special attention. Ring 4, being the most oblique ring of beams, necessitates beam ellipticity to irradiate the equator effectively. The blue curve in Fig. 6 shows the position of the outer shell surface relative to the mean, versus polar angle with only circular beam profiles. The equator is significantly under-driven. This cannot be remedied with higher laser power for the equatorial ring. This is because a circular beam profile for ring 4 with a 5% radius equal to the target radius results in energy being deposited to a polar angle of nearly 30^{o}. (An elliptical profile with a 5% semi-major axis equal to the target radius has a 5% semi-minor axis less than this radius and thus does not spread energy deposition as widely in the polar direction.) Thus it is difficult to sufficiently drive the equator without dangerously over-driving higher latitude portions of the target.

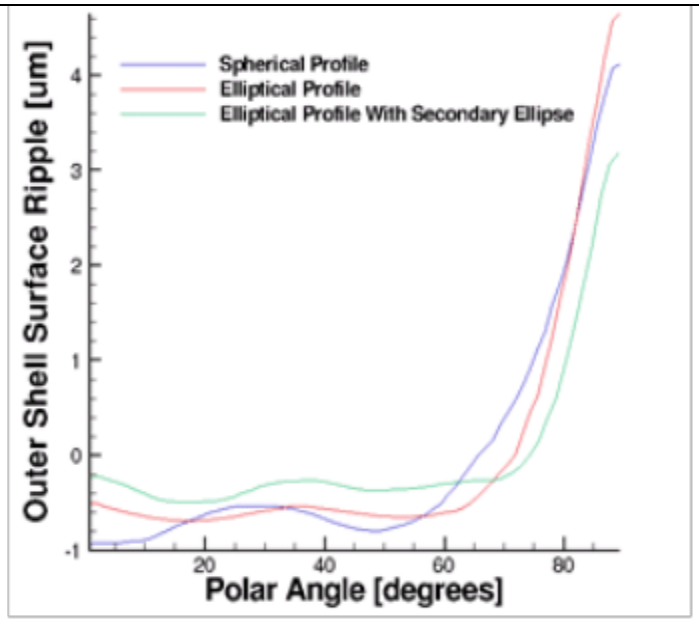

Figure 6: Outer shell surface position relative to the mean at 2 ns for optimized implosions using three different beam profiles for ring 4.

Localizing the energy distribution at the equator via use of an elliptical beam profile is doubly advantageous. First, this localization with respect to polar angle directly increases the amount of energy deposited at more-equatorial latitudes, providing greater drive. Second, it allows any laser power increases for ring 4 to preferentially drive the equator without overdriving the higher latitudes. The curves in Fig. 6 illustrate these effects. The case which uses ellipticity for ring 4 (red curve) shows a better-driven equatorial region (the range 60° to 75° is in particular improved), and a flatter surface northwards of 60°. Adding a secondary ellipse with an offset [Fig. 3c and Eq. (1.3)] iterated upon the benefits of this localization by further localizing the intensity and shifting the center of localization away from higher latitudes (green curve in Fig. 6).

The neutron yield from the fusion of deuterium ions is a good measure of target performance. Neutron yield can be increased by increases in drive velocity; however, when

two implosions have comparable velocities and incident energies, differences in uniformity can result in differences in neutron yield. As the target converges near the end of an implosion, the fuel becomes concentrated in a hot, dense area bound by the plastic shell and known as the hot spot. A more uniform implosion will feature a more uniform (close to spherical) hot spot, and higher hot spot uniformity generally leads to a higher neutron yield. The case featured in Fig. 6 using an elliptical profile for ring 4 has a 5.5% higher yield than the case using a circular profile, and adding the secondary ellipse brings a further 18.5% increase in yield compared to the case using a purely elliptical profile. Clearly, the equator was not sufficiently driven in any simulation, but the improvements brought by utilizing an elliptical beam profile which includes a secondary ellipse are encouraging.

Gaussian order is an additional parameter which can affect the overall shape and effect of a beam profile. Profiles with a lower Gaussian order are more sharply peaked, whereas higher-order profiles spread intensity out over a larger region. For this reason, lower Gaussian orders are more optimal for more equatorial rings as their localization can compensate somewhat the effects of obliquity. Therefore, in an optimal set of beam profiles, the order for each ring should get consistently lower moving from pole to the equator, i.e, from the less displaced to the most displaced rings of beams.

III. Results

An optimal set of beam profiles was identified using the trends outlined in section II. Optimal beam profile parameters and the corresponding optimal pulse shapes are shown in Tables II and III and Fig. 7 respectively. The beam profile of ring 4 includes a moderate degree of ellipticity and a secondary ellipse, while the other rings have circular or close to circular beam profiles. Gaussian orders also decrease as was described previously. These

Ring	1	2	3a	3b	4
Gaussian Order	4.4	2.7	3.2	2.4	2.0
Ellipticity	1.0	1.0	1.0	1.2	1.6

Table II: Beam profile parameters used to obtain the uniform implosion shown in Figs. 8 and 9b.

Relative Amplitude of SE	0.5
Gaussian Order of SE	2.0
Relative offset of SE	0.15
Ellipticity of SE	2.1

Table III: Parameters of the Secondary Ellipse (SE) present in the profile used for ring 4. Offset is relative to the radius of the target

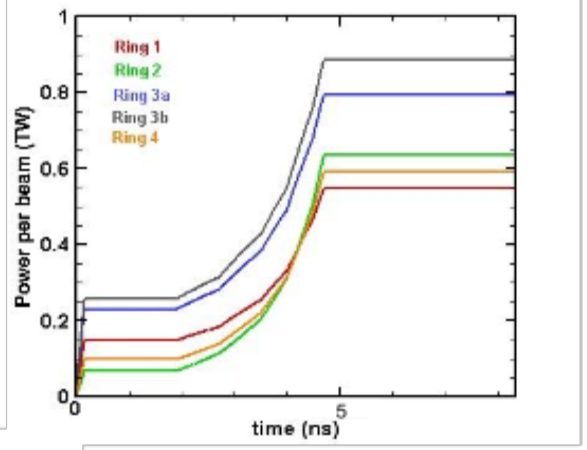

Figure 7: Pulse shapes for all 5 rings for optimized case. Note that the ratio between the Powers of Ring 3a and 3b must remain constant throughout the implosion

optimized profiles and parameters achieve an implosion with high levels of uniformity, as is detailed below in Figs. 8 and 9b.

Note that while section II suggested that more oblique rings' profiles should have higher Gaussian orders and that rings 1-3b should have circular profiles, the super-Gaussian order for the rings does not monotonically decrease with increasing polar angle, and Ring 3b has a small ellipticity of 1.2. These deviations come from a specific constraint applied to the pulse shapes for rings 3a and 3b. As is seen in Fig. 1, ring 3 is split into rings 3a and 3b for polar drive. Due to the organization of beam lines on the NIF, the pulse shapes for rings 3a and 3b must be the same, although an energy ratio close to 1.0 between the two rings is tolerable. For the optimal pulse shapes shown in Fig. 7, the pulse shape of ring 3b has a 12% higher energy than the pulse shape of ring 3a. This constraint on the pulse shapes for rings 3a and 3b reduces

control over symmetry in the 40° - 70° region where these rings are most influential. Generally, due to the increased obliquity, more energy is required around 70°, or where ring 3b is most influential. The ellipticity in the profile for ring 3b helps to localize energy there, and the higher super-Gaussian order for ring 3a lessens the drive near the 45° region and instead spreads energy out to regions which include the 70° area. These choices of beam profile help to restore symmetry which could otherwise be compromised by the pulse shape constraint for rings 3a and 3b.

In designing uniform ICF implosions, it is vitally important to maintain a high degree of uniformity until shock breakout, which occurs around 2 ns for this pulse shape. Non-uniformities introduced early on in an implosion will tend to grow as time continues, and, in particular, non-uniformities in the shock which is launched at the initial time of laser irradiation can give rise to hot spot non-uniformities near the time of peak compression which compromise target performance. The implosion whose parameters are described in Fig. 7 and Tables II and III has a shock strength that is very uniform, as is shown in Fig. 8.

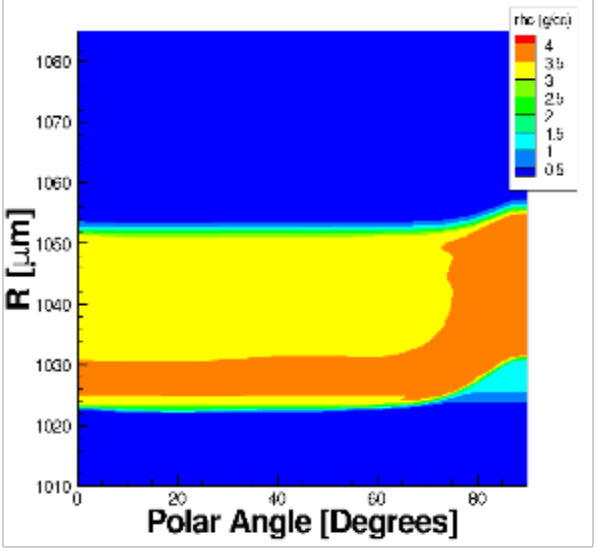

Figure 8: Density contour at shock breakout for optimized implosion. 0° corresponds to the pole, while 90° corresponds to the equator

Optimizing past shock breakout is generally accomplished by optimizing the power of each ring during the main pulse. The late-time results of the implosion shown in Fig. 8 are shown in Fig. 9b, which shows mass density contours at peak neutron production, when the target has converged by roughly a factor of 10 from the initial radius. Mass density contours from a simulation of current NIF implosions with existing NIF indirect-drive

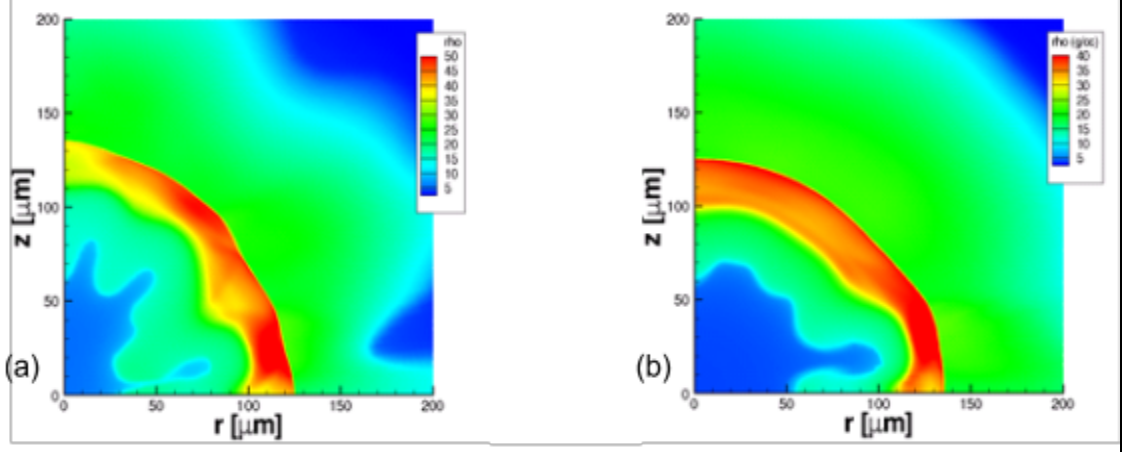

Figure 9: Density contours at a convergence ratio of 10 (8.1 ns) for (a) an optimized implosion using current NIF beam profiles and (b) an implosion which uses the optimized set of beam profiles identified in Tables I and II

beam profiles are shown in Fig. 9a next to those of the simulation with optimized beam profiles shown in Fig. 9b. The inner fuel-shell interface (shown by the contours separating the blue and green regions inside the shell) for the simulation of the implosion which uses the optimized set of beam profiles has a much higher degree of uniformity than that of the simulation which uses the existing set of beam profiles. Quantitatively, table IV shows that the distortion of this interface for the implosion shown in Fig. 9a is twice as high as that of the implosion in Fig. 9b which uses an optimized set of beam profiles. Table IV also compares the neutron yields of these two implosions, and shows that use of the optimized set of beam profiles increases the neutron yield by more than 50%.

	Current NIF beam profiles	Optimized beam profiles
Hot Spot Distortion	12.5%	6.2%
Neutron Yield	1.7×10^{12}	2.6×10^{12}

Table IV: Target performance for implosions visualized in Fig. 9a and 9b, (columns 2 and 3 respectively). Hot spot distortion is defined as the ratio of the rms of the inner fuel-shell interface to the average radius of the interface.

When modeling implosions with a simulation code such as DRACO, there are questions as to the accuracy of certain aspects of this modeling. In some cases, multiple models exist for one aspect of the hydrodynamic simulation. One example is heat conduction, and uncertainty in the heat conduction model is one model variation that can be explored. Since the corona of the NIF has temperatures of ~4 keV, the electrons that conduct heat have energies ~20 keV and large mean-free paths that permit them to reach the ablation surface. Heat conduction is typically modeled using diffusion, which assumes small electron mean free paths; however, it is expected that the non-local effects of large mean-free paths will alter the drive at the ablation surface.

Because the phase plates which determine beam profiles are fixed and expensive, it is desirable that a set of beam profiles optimized and shown to be successful (compared to current NIF profiles) with one heat conduction model not have that success compromised by the use of alternate models. The optimal set of profiles previously identified was used in

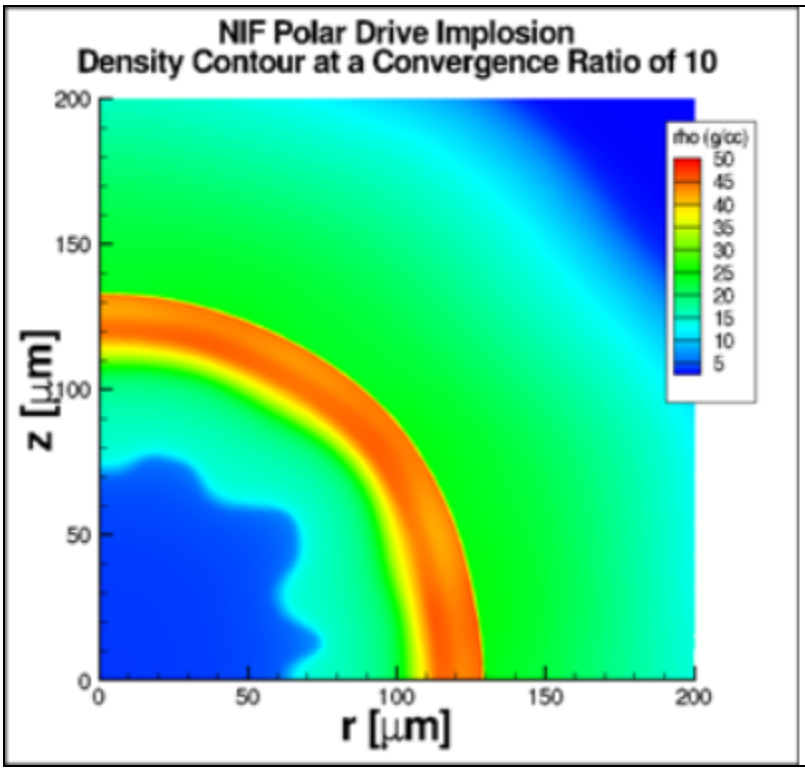

Figure 10: Mass density contours at a convergence of ~10 for a simulation with the optimal beam profiles and a non-local heat conduction model.

simulations with a non-local heat conduction model instead of a flux-limited model as is used in the majority of this work. Excellent symmetry was recovered with minor changes to the ring laser pulse shapes for the same set of beam profiles. (Fig. 10)

IV. Conclusion

Current experiments on the National Ignition Facility which explore the use of direct drive ICF via polar drive use a set of phase plates designed for indirect drive. Simulations were carried out using the 2D hydrodynamics code DRACO which aimed to identify an optimal set of beam profiles and compare the performance of these profiles to that of the current NIF profiles. By varying Gaussian orders and ellipticities and exploring the use of secondary ellipses, and ultimately by fine tuning pulse shapes, a set of optimal beam profiles was identified which had the capability to significantly improve the uniformity of a polar drive implosion, increasing the simulated fusion yield by more than 50%, and whose benefits are robust to variations in the heat conduction model.

V. Acknowledgements

I would like to extend thanks to the amazing people who contributed to the successful completion of this project and this report and who made my all too brief summer sojourn at LLE one of the greatest experiences I've had. I'd like to thank every member of the lab in addition to all the participants in this year's high school program for creating such a fantastic environment to work in. In particular, I'd like to thank Dr. Stephen Craxton, for providing me with the opportunity to carry out this research and for doing so much work to give other high

school students this experience every year, Michael Charissis, for providing me with the technical support necessary for this project, and Ian Gabalski, for sharing with me so much of his knowledge, work, and expertise in this area of study. I'd especially like to thank my advisor, Dr. Radha P. Bahukutumbi. She poured a huge amount of effort into both creating this project and guiding me through it, and did a fantastic job providing me with the perfect amount of guidance to make this project such a success.

References

1. J. Nuckolls, L. Wood, A Thiessen, and G. Zimmerman, Nature 239, 139 (1972).
2. S. Atzeni and J. Meyer-ter-Vehn, *The Physics of Inertial Fusion: Beam Plasma Interaction, Hydrodynamics, Hot-Dense Matter*, International Series of Monographs on Physics (Clarendon, Oxford, 2004).
3. J. D. Lindl, Phys. Plasmas 2, 3933 (1995).
4. T. R. Boehly et al., Opt. Commun. 133, 495 (1997).
5. J. D. Lindl and E. I. Moses, Phys. Plasmas 18, 050901 (2011).
6. S. Skupsky et al., Phys. Plasmas 11, 2763 (2004).
7. P. B. Radha et al., Phys. Plasmas 20, 056306 (2013).
8. T. J. B. Collins et al., Phys. Plasmas 19, 056308 (2012).
9. P. B. Radha et al., Phys. Plasmas 12, 032702 (2005).